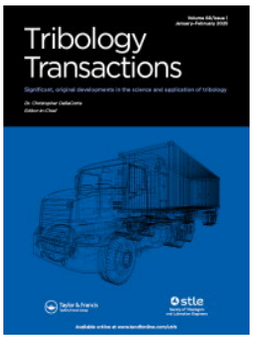

Tribology Transactions

ISSN: (Print) (Online) Journal homepage: www.tandfonline.com/journals/utrb20

Improvement of Surface Properties and Wear Resistance of Selective Laser Melting-Fabricated Inconel 625 Alloy by Ultrasonic Nanocrystal Surface Modification for Demanding Applications

Zahra Fathipour, Morteza Hadi, Omid Bayat & Filipe Fernandes

To cite this article: Zahra Fathipour, Morteza Hadi, Omid Bayat & Filipe Fernandes (28 Feb 2025): Improvement of Surface Properties and Wear Resistance of Selective Laser Melting-Fabricated Inconel 625 Alloy by Ultrasonic Nanocrystal Surface Modification for Demanding Applications, Tribology Transactions, DOI: 10.1080/10402004.2025.2457970

To link to this article: https://doi.org/10.1080/10402004.2025.2457970

TRIBOLOGY TRANSACTIONS
https://doi.org/10.1080/10402004.2025.2457970

Improvement of Surface Properties and Wear Resistance of Selective Laser Melting-Fabricated Inconel 625 Alloy by Ultrasonic Nanocrystal Surface Modification for Demanding Applications

Zahra Fathipour[a], Morteza Hadi[a], Omid Bayat[b], and Filipe Fernandes[c,d]

[a]Materials Engineering Group, Golpayegan College of Engineering, Isfahan University of Technology, Golpayegan, Iran; [b]Department of Metallurgy and Materials Engineering, Hamedan University of Technology, Hamedan, Iran; [c]CIDEM, ISEP – Polytechnic of Porto, Porto, Portugal; [d]Department of Mechanical Engineering, CEMMPRE, ARISE, University of Coimbra, Coimbra, Portugal

ABSTRACT

Inconel 625 alloy is widely utilized in the production of components for demanding industries. This study investigates the effect of ultrasonic nanocrystal surface modification (UNSM) on the surface properties and wear resistance of Inconel 625 alloy produced by selective laser melting (SLM). Specifically, it focused on analyzing the effect of UNSM on the microstructure, hardness, surface roughness, coefficient of friction and essentially wear resistance of the alloy. The results showed that the microstructure formed by SLM, characterized by relatively large melt pools, was modified by UNSM to a depth of approximately 10 to 15 microns, resulting in a new microstructure composed of deformed grains without changing the chemical composition. Surface hardness increased by over 63% after UNSM treatment. In addition, the surface roughness initially induced by the SLM process was reduced by more than 90%, resulting in a tenfold reduction in the coefficient of friction. Wear path analysis showed that while the abrasive wear mechanism of the alloy remained unchanged, the UNSM treated samples exhibited increased debris production and more frequent delamination due to reduced workability. The alterations in surface properties, including reduced crystallite size, increased lattice strain, grain refinement, and decreased surface area, have been identified as key contributors to the enhanced hardness and wear resistance of the alloy following UNSM treatment.

ARTICLE HISTORY
Received 16 October 2024
Accepted 15 January 2025

KEYWORDS
Inconel 625; ultrasonic nanocrystal surface modification; selective laser melting; wear rate; nickel-based superalloy

Introduction

Inconel 625 is a nickel-chromium-molybdenum superalloy that contains additional alloying elements, such as niobium. This superalloy is well-known for its outstanding properties, which include high yield strength, tensile strength, and creep resistance. (*1*) It also exhibits exceptional corrosion resistance, even in harsh environments over extended periods, as well as resistance to oxidation at elevated temperatures. (*2*,*3*) Inconel 625 also offers excellent machinability and weldability, positioning it as an optimal choice for a variety of applications. (*4*) Due to its comprehensive properties and the capability to function effectively at both low and high temperatures, the application areas of Inconel 625 are diverse, spanning the chemical and petrochemical industries as well as the aerospace sector. (*1*,*4*)

Inconel 625 alloy parts are currently produced through casting, forming, and machining. However, due to the challenges associated with the manufacturing processes of such superalloys, they have increasingly become a prominent candidate for additive manufacturing in recent years. (*5*,*6*) In addition to mitigating certain issues during production through conventional methods, the additive manufacturing process offers the advantage of reducing the buy-to-fly ratio for these components. This consideration is particularly significant given the relatively high cost of this alloy. (*7*) Among the production methods utilizing additive manufacturing, the selective laser melting (SLM) method offers distinct advantages. These include enhanced dimensional accuracy, the potential for achieving higher density, the capability to manufacture larger parts with complex geometries, and it has garnered significant interest from researchers. (*6*,*8*)

Despite the advantages of additive manufacturing, limitations such as suboptimal surface finish, noticeable surface tensile stress, and considerable surface porosity impede its application. (*9*) The issue of roughness control in SLM components has been extensively researched, with studies addressing the non-uniformity of surface roughness in these parts. (*10*) Research indicates that surface roughness, porosity, and residual tensile stresses have a direct impact on the reduction of fatigue life in SLM components. (*11*) Consequently, methods for stress relief or surface roughness reduction are critically necessary in this field. To simultaneously address all three of these disadvantages, researchers have focused on the application of severe surface plastic

CONTACT Morteza Hadi m.hadi@iut.ac.ir
Review led by K. Khanlari.

deformation, which has the potential to enhance wear resistance, improve surface quality, and eliminate tensile residual stresses. (*12*,*13*)

The severe surface plastic deformation process entails the application of force to induce lattice strain within a defined thickness of the sample's surface. This procedure alters the microstructure and crystal structure, ultimately leading to an improvement in the material's properties. (*14*) Studies have demonstrated that this modification can enhance hardness, wear resistance, fatigue resistance, and corrosion resistance. (*15*,*16*) Several surface plastic deformation techniques have been developed, including laser shock peening (LSP), (*17*,*18*) shot peening (SP), (*19*,*20*) and ultrasonic nanocrystal surface modification (UNSM). (*21*–*23*) These techniques are designed to generate compressive residual stresses on the surface of the sample, thereby enhancing its mechanical properties. (*24*)

Based on previous and ongoing research, UNSM is a potentially effective post-processing technique for enhancing the performance of additively manufactured components. (*25*,*26*) It enhances the microstructural properties of the surface, decreases surface roughness, and induces compressive residual stress. The UNSM treatment influences the metal surface through the generation of high-frequency vibrations via ultrasonic energy. These vibrations are transmitted to a tool tip composed of a hard material such as tungsten carbide, which then interacts with the surface. (*27*) Simultaneously, the tool tip exerts a fixed static force onto the surface. This method of force application generates high energy impacts at the surface, leading to significant plastic deformation. (*28*)

To date, various studies have focused on improving the surface quality of steels, (*29*,*30*) aluminum alloys, (*31*) titanium alloys, (*22*) AZ91 magnesium alloy, (*32*) cobalt-chromium-molybdenum (Co-Cr-Mo) alloy, (*33*) silicon carbide, (*34*) Cu-based alloy, (*35*) and nickel-based alloys (*36*–*38*) using the UNSM method. In most of these studies, a significant improvement in the properties of the alloy under investigation has been observed, accompanied by a favorable evaluation of the surface modification process. For nickel-based alloys, Li et al. (*39*) investigated the relationship between grain size and hardness in Inconel 690 alloy following UNSM treatment. Their findings revealed that a decrease in grain size was associated with an increase in hardness. In a separate study conducted on the same alloy, it was observed that UNSM enhanced dislocation density, leading to the formation of a nanostructured surface on the alloy. (*40*) Kattoura et al. (*41*) studied the effects of UNSM on the Inconel 718 Plus alloy. Their findings demonstrated that UNSM significantly improved fatigue life by inducing near-surface microstructural changes, generating high residual compressive stress, and enhancing surface hardening.

Issues related to surface roughness, porosity, and surface tensile stress have been documented for Inconel 625 alloy produced via SLM. (*42*) Furthermore, research has indicated that the surface properties of this alloy can be enhanced through techniques such as shot peening and laser shock peening. Despite these studies and the significant importance of Inconel 625, no research has been conducted on the changes in surface properties of this alloy caused by UNSM. Given the use of Inconel 625 in harsh chemical environments, such as marine applications, and its relatively low hardness, wear and friction are critical to extending the life of moving mechanical components. This is particularly important for Inconel 625 manufactured using the SLM process, which tends to have relatively high roughness due to the manufacturing process. Therefore, this study investigates the extent to which the UNSM treatment alters the surface properties of Inconel 625 alloy produced by the SLM process, including microstructure, hardness, roughness, and wear resistance. The results of this study can help determine the specific type and degree of influence the UNSM treatment has on these essential functional properties of Inconel 625 alloy.

Experimental details

In this study, samples of Inconel 625 alloy were produced using a selective laser melting machine. Gas atomized Inconel 625 powders (>65 µm) were used, with a powder layer thickness of 30 µm during the SLM process. The samples were additively manufactured as rectangular blocks, each with dimensions of 60 mm × 10 mm × 6 mm, using a maximum laser power of 300 watts. SLM parameters have been extensively studied, and in this work, we applied the optimal parameters reported in the literature. (*43*) The chemical composition of the alloy produced was verified to conform to the standard Inconel 625 specification.

The UNSM treatment involved applying ultrasonic vibrations to a tungsten carbide ball in contact with the alloy surface. This was done at a frequency of 20 kHz, under a static load of 70 N, with an ultrasonic amplitude of 30 µm and a scan speed of 2,000 mm/min. Scans were taken at 1 mm intervals. The UNSM parameters have been optimized in previous studies, and the deviation of these parameters is not significant. In this paper, the UNSM parameters have been selected based on a study that reported notable achievements following treatment. (*44*)

Following the UNSM treatment, the hardness of both unmodified and modified samples was measured using a Vickers hardness tester. The test was conducted with a load of 3 kg and a dwell time of 15 s. The hardness values reported are the average of at least five measurements. For microstructural examination, the specimens were polished to 2,000 grit on their cross-sections. The polished samples were then etched for 5 s in a solution of 95 mL hydrochloric acid and 5 mL hydrogen peroxide. The microstructural features were analyzed using an optical microscope and a scanning electron microscope.

Surface roughness was assessed by measuring Ra and Rz using a surface roughness tester. Ten measurements were taken for each specimen to determine average roughness values. A reciprocating wear tester was used to assess the coefficient of friction and wear performance. The wear tests were performed at room temperature under dry sliding conditions utilizing 1.3 mm diameter tungsten carbide pins.

Two different loads (10 N and 20 N) were applied at a constant sliding speed of 7 cm^3/s. The repeatability of the wear tests was assessed through three trials, revealing deviations of less than 2% in both weight loss and friction coefficient. After the tests, the wear paths were analyzed using a scanning electron microscope.

Mass loss, measured in milligrams per 50 m of sliding distance, was calculated using the following equation:

$$M = m_i - m_f \quad [1]$$

where M represents the mass reduction, m_i is the initial mass, and m_f is the final mass. The wear rate was determined using the following equation:

$$W_R = \frac{M}{\rho LN} \quad [2]$$

In this equation, W_R is wear rate in mg/Nm, ρ is the density of the Inconel 625 alloy (mg/mm^3), L is the sliding distance (meters) and N is the normal force applied to the pin (Newtons).

X-ray diffraction (XRD) analysis was conducted using a Cu-Kα radiation source ($\lambda = 1.5418$ Å) under operating conditions of 40 kV and 35 mA. The scanning angle varied from 20° to 80°, with a scanning speed of 0.1° per minute. The phases present in the surface layers of both unmodified and modified samples were identified by comparing the diffraction patterns with standard reference patterns from the International Center for Diffraction Data (ICDD). Differences in peak positions and widths were carefully analyzed. The Williamson-Hall method was then used to determine crystallite size and lattice strain.

Results and discussions

Figure 1 shows the initial microstructure of the SLM alloy in its as-built state and the microstructure of the alloy after UNSM treatment. Examining this figure, the initial microstructure of the alloy consists, as expected, of melt pools resulting from the solidification of the regions scanned by the laser beam (Fig. 1a). In these melt pools fine grains are formed due to the rapid solidification process. These grains are difficult to see at the resolution achievable in the light microscope but can be seen more clearly at higher magnifications in the scanning electron microscopy (SEM) images (Fig. 1b–d). The gradual increase in magnification of the images of the SLM alloy from Fig. 1b to d allows the identification of two distinct features. First, the presence of large melt pools with columnar growth resulting from directional solidification can be seen in the microstructure of the SLM alloy. Second, the presence of numerous grains can be observed. The effect of rapid freezing on the grain size within these melt pools is clearly visible. From Fig. 1e, the UNSM treatment has resulted in the compaction of a layer of the sample surface because of the ultrasonic vibrations. As a result, the boundaries of the melt pools are no longer visible in this area. Previous studies have shown that during the plastic deformation of metals using the SLM process, the structure of the molten pools is maintained, and deformation occurs as these pools are deformed. (*45*) Put simply, the overall shape of these pools is maintained during normal plastic deformation and does not collapse completely. The removal of these melt pools indicates that severe plastic deformation has occurred on the surface of the UNSM metal. SEM images confirm that the columnar microstructure resulting from SLM has been completely removed to a thickness of approximately 10 to 15 µm (Fig. 1f and g). Previous studies have indeed addressed the gradient nature of the changes induced by the surface impact of ultrasonic vibrations. (*46*) Due to this nature, it is not possible to determine with certainty the thickness of the layer affected by UNSM. However, it can be assumed that the intensity of the plastic deformation has caused a minimum thickness to be severely affected. Figure 1h presents the microstructure within the UNSMed region at high magnification, akin to the depiction in Fig. 1d from the SLM region. A comparison of these figures reveals a reduction in grain size in the superficial UNSMed region. This finding suggests that the ultrafine grain structure of the SLM alloy has refined further because of the UNSM treatment, achieving a size of approximately 100 nm. Research on the 316 L alloy has demonstrated that UNSM treatment induces a substantial number of dislocations due to severe surface plastic deformation. The interaction among these dislocations facilitates the formation of dislocation cells, which progressively develop into sub-boundaries, leading to a significant reduction in grain size and an increase in the density of grain boundaries within the sample. (*47*)

Figure 2 also displays the energy-dispersive X-ray spectroscopy (EDS) elemental analysis of the deformed region on the surface and a region within the substrate metal marked in Fig. 1g. A comparison of the results obtained in areas A and B confirms that the plastic deformation at the surface has not altered the chemical composition. The slight discrepancy observed between the two analyses, given the quantitative accuracy of the EDS analysis, supports the conclusion that the UNSM treatment did not cause any changes in chemical composition. Rather, it only affected the microstructural form.

Figure 3 illustrates the Vickers hardness results for Inconel 625 alloy samples in two different conditions: as-built and UNSM. The figure clearly demonstrates that the average hardness of the samples has increased significantly, rising from approximately 304 Vickers to approximately 497 Vickers. This change demonstrates a significant increase in hardness after the UNSM treatment, with a 63.3% improvement. Additionally, the figure showcases an example of the indentation image for each condition. The contrasting sizes of the indentations further highlight the substantial difference in hardness between the two samples, with the UNSM sample exhibiting greater hardness and a smaller indentation.

The increase in hardness is due to the impact of ultrasonic vibrations and the severe plastic deformation of the surface during the surface modification process. This causes fine graining and work hardening of the surface layer of the Inconel 625 alloy. In Fig. 1, it was found that the UNSM

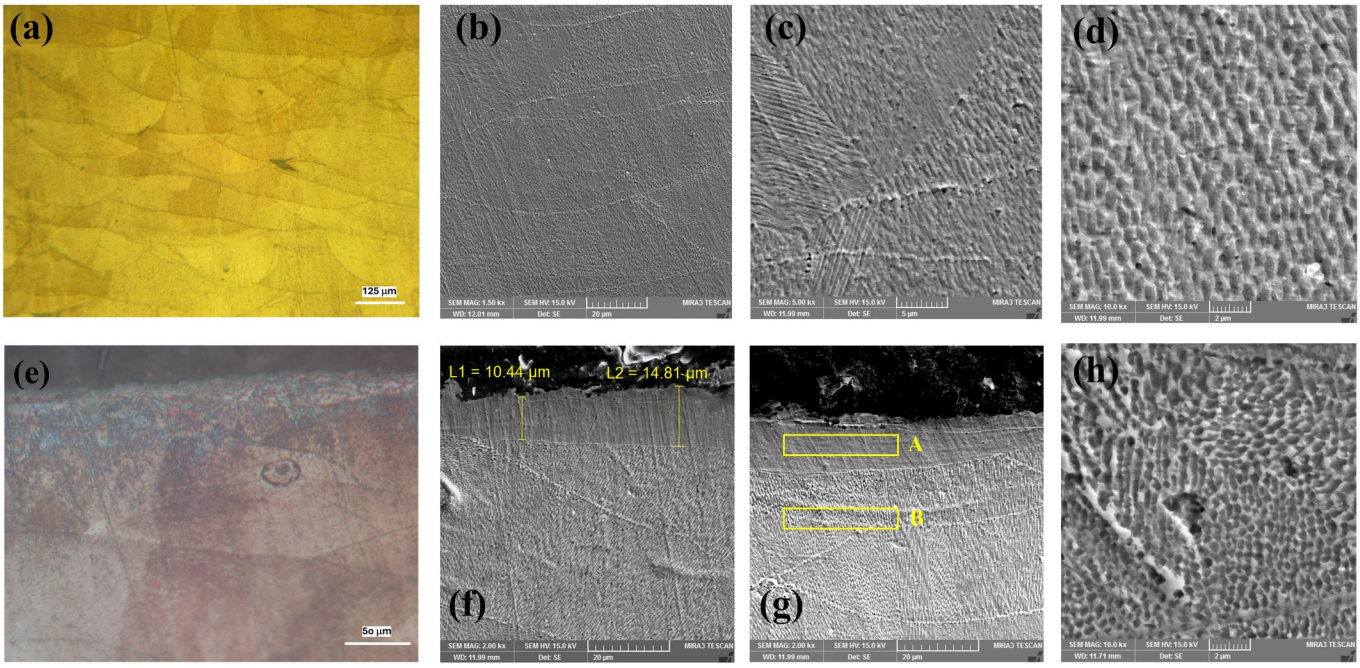

Figure 1. Microstructural image of the alloy in the as-built condition with an optical microscope (a) and with a scanning electron microscopy (SEM) at magnifications of 1,500 times (b), 5,000 times (c), and 10,000 times (d). Also included are microstructural images of the alloy after ultrasonic nanocrystal surface modification (UNSM) with an optical microscope (e) and with a SEM at two different points on the surface (f and g), and finally a high-magnification SEM image from the UNSM treated layer marked by A (h).

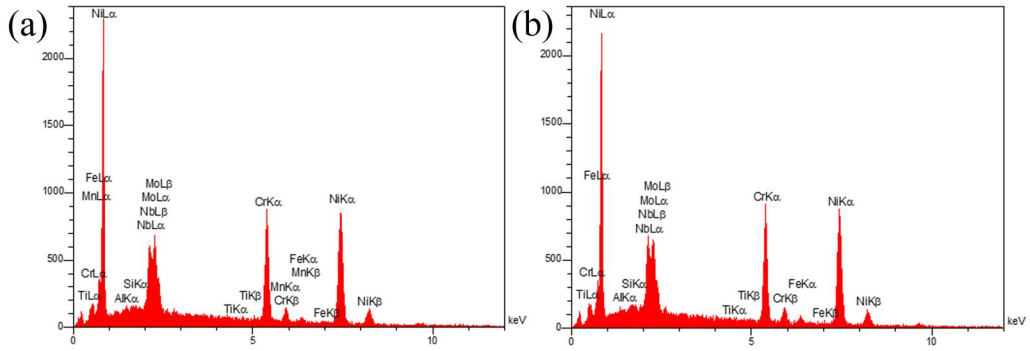

Elt	W%	A%
Al	0.00	0.00
Si	0.18	0.39
Ti	0.00	0.00
Cr	18.66	22.36
Mn	0.00	0.00
Fe	0.78	0.87
Ni	58.10	61.67
Nb	10.77	7.22
Mo	11.52	7.48
	100.00	100.00

Region A

Elt	W%	A%
Al	0.00	0.00
Si	0.27	0.59
Ti	0.05	0.06
Cr	18.65	22.33
Fe	1.10	1.23
Ni	57.54	61.02
Nb	11.33	7.59
Mo	11.07	7.18
	100.00	100.00

Region B

Figure 2. Energy-dispersive X-ray spectroscopy (EDS) analysis from regions a and B marked in Fig. 1(g) represents the ultrasonic nanocrystal surface modification (UNSM)-treated (a) and non-treated (b) zones.

surface treatment caused a layer on the surface to undergo severe plastic deformation, reaching a depth of approximately 15 micrometers. The application of cold work in metals typically reduces the mobility of dislocations. Therefore, it appears that the plastic deformation resulting from the UNSM treatment has led to an increase in

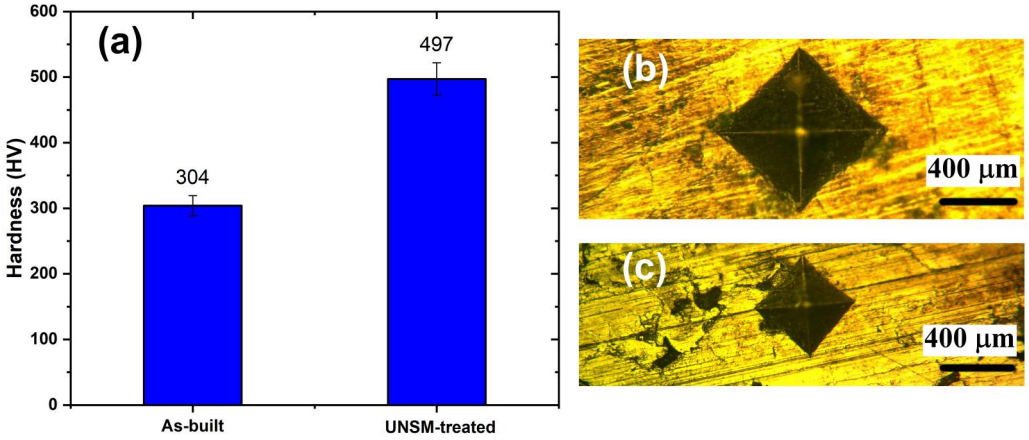

Figure 3. Comparison of the hardness value of the surface of the sample in the as-built condition and in the ultrasonic nanocrystal surface modification (UNSM)-treated condition (a) and an example of the image of the indentation made in the as-built sample (b) and the UNSM sample (c).

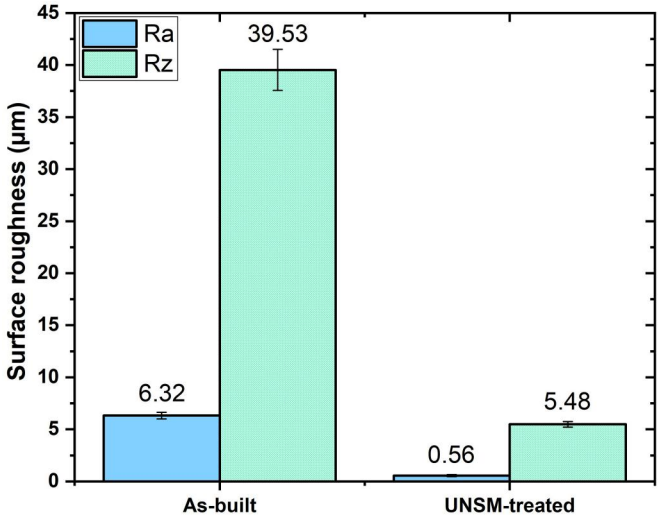

Figure 4. Surface roughness of Inconel 625 alloy expressed by the two parameters Ra and Rz under ultrasonic nanocrystal surface modification (UNSM) modified and unmodified conditions.

hardness for the treated sample. In fact, the severe plastic deformation that occurs at the surface increases the dislocation density, which hinders dislocation movement and consequently increases hardness. Recent studies on 316 L steel have demonstrated comparable outcomes following UNSM, with the increased yield strength primarily attributed to a reduction in grain size and a high density of dislocations and deformation twins. (*47*) The increase in lattice strain caused by the UNSM treatment, which will be discussed further when the XRD results are examined, may also have contributed to the observed increase in hardness.

Figure 4 shows the results of the roughness measurements in terms of Ra and Rz. From this figure it can be seen that because of the surface modification, the mean value of roughness has been reduced from 6.320 to 0.558 microns, indicating a 91.2% reduction in surface roughness. The significant difference in the Rz value (a reduction of 86.1%) also confirms that the surface is much smoother, with less height variation and greater uniformity after ultrasonic nanocrystal surface modification. During the UNSM treatment, a compressive effect is created on the sample surface. This is achieved by applying a static load to the ball-shaped tip of the UNSM instrument. The ball tip scans the alloy surface in a similar way to grinding. Therefore, tapping the surface while simultaneously scanning causes severe plastic deformation of the top layer of the alloy. This action effectively eliminates the ridges and smooths the rough peaks by pushing them into the valleys. This mechanism has previously been described to explain the effect of the UNSM treatment on roughness reduction. (*48*) Similarly, it has been reported that the reduction in roughness of the 316 L SLM-produced alloy is attributed to the compression effect generated by the high-frequency impacts from the UNSM tip. This impact induces plastic flow on the material's surface, effectively leveling the roughness peaks into the valleys and resulting in a smoother surface finish. (*47*) The use of ultrasonic vibrations for surface modification is a widely recognized technique. Based on the surface roughness of the samples produced by SLM, the use of this method can effectively improve the surface roughness of alloys. (*49*) This issue has previously been investigated for Ti-6Al-4V, (*50*) Co-Cr-Mo, (*33*) and 316 L (*51*) alloys. It has also been found that the effectiveness of UNSM in altering roughness is greater than that of shot peening. (*52*) However, this research is the first to report the influence of UNSM on the roughness of Inconel 625 alloy produced by SLM.

Previous studies on other materials have shown that a smoother surface can improve the fatigue life of the alloy by reducing stress concentrations that act as crack initiation sites. (*44*) In addition, an improved surface finish contributes to better corrosion resistance by minimizing the number of sites where corrosive agents can penetrate. (*53*) Smoother surfaces also generally result in less friction and wear, (*35,53*) which is critical for components used in high performance applications such as aerospace and marine. In the following, we will focus on investigating the changes in friction and wear properties of SLM-produced Inconel 625 in its as-built condition and after ultrasonic modification.

Figure 5 illustrates the changes in the coefficient of friction calculated during the wear test in two conditions: UNSM treated and as-built, and at two different forces (10 and 20 Newtons). As shown in this figure, the average

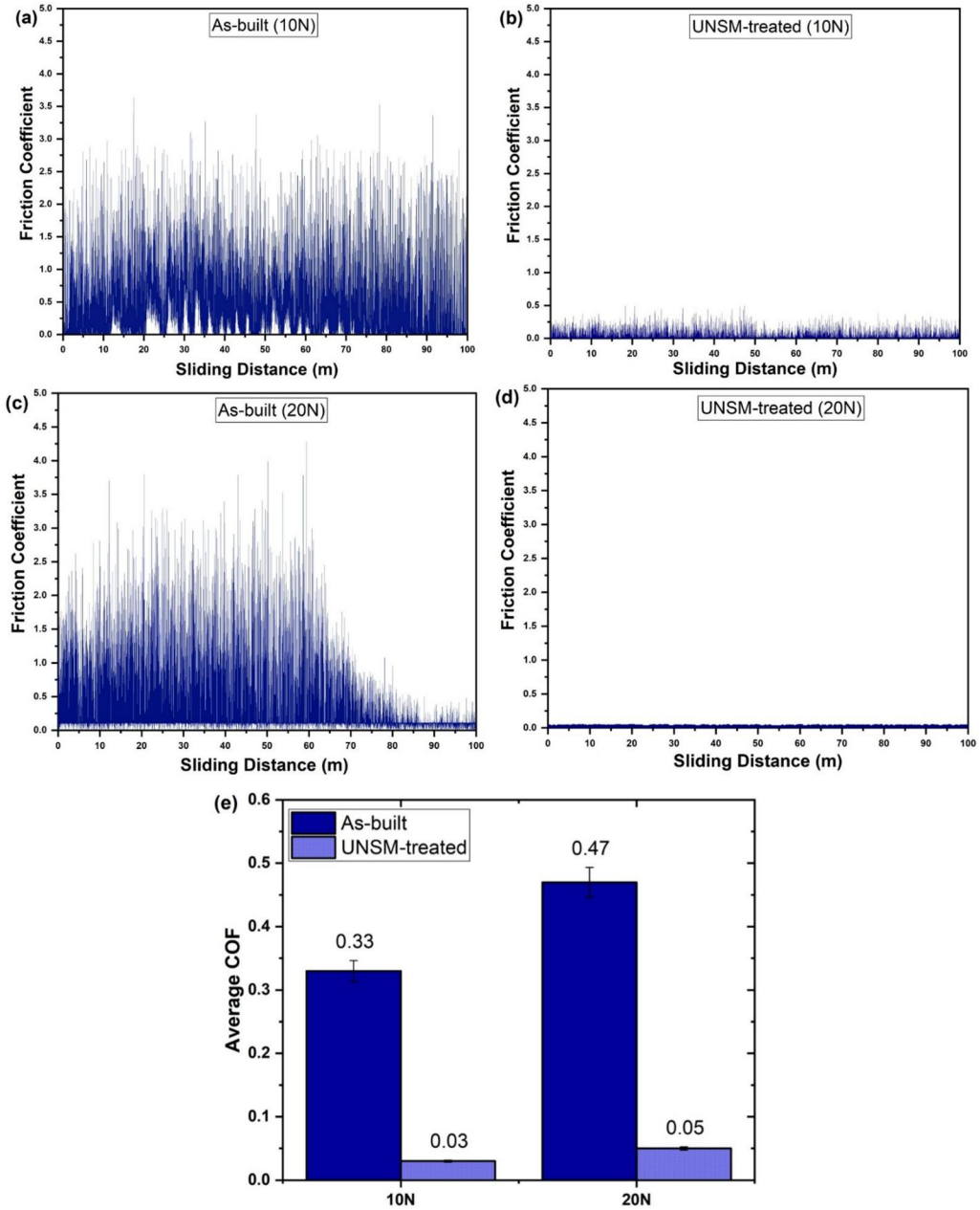

Figure 5. Coefficient of friction plotted against distance, showing the results for the as-built condition (a) and the ultrasonic nanocrystal surface modification (UNSM) treated condition (b) under a test load of 10 Newtons, and for the as-built condition (c) and the UNSM treated condition (d) under a test load of 20 Newtons. The average coefficient of friction for these conditions is also shown (e).

friction coefficient in the UNSM sample has decreased significantly in both the 10 N and 20 N modes. For better comparison, Fig. 5e compares the average friction coefficient values for these four cases. The interesting aspect of the results from two different forces is that the reduction in the coefficient of friction after the UNSM treatment is almost identical for both forces, approximately 10 to 1. This illustrates that the UNSM treatment consistently reduces the coefficient of friction regardless of the force applied. The main reason for reducing the coefficient of friction using the UNSM treatment is that it reduces surface roughness by applying ultrasonic vibrations. This process effectively eliminates the ridges and valleys that form on the surface because of the SLM process, ultimately improving smoothness. In other words, the reduction in roughness, whose quantitative values are shown in Fig. 4, contributes directly to the reduction in the coefficient of friction. Additionally, studies indicate that the UNSM treatment can effectively eliminate surface pores, (*51*) potentially enhancing the reduction of the coefficient of friction. This is particularly significant given that gas porosity, which arises from the gas atomization powder production process, is present in SLM parts, albeit in minimal quantities. (*54*)

In addition, Fig. 5 shows that the fluctuations in coefficient of friction values are significantly greater for as-built samples compared to UNSM treated samples. It is evident that the reduction in surface roughness leads to a decrease in the fluctuations of the coefficient of friction in the UNSM specimen. In addition, the higher wear resistance in the UNSM specimen, which will be further investigated in the

remainder of this article, may also play a role in reducing the coefficient of friction fluctuations. Previous studies on other alloys have demonstrated that elevated wear rates can result in an increased likelihood of local layer failure, scratching, and heightened surface roughness. (*55*,*56*) These factors can effectively amplify the fluctuation in the coefficient of friction. Therefore, it is evident that the UNSM treatment has successfully reduced both the average friction coefficient and the fluctuation of this value across the surface. This is particularly important because high roughness and varying friction coefficients in SLM samples can be limiting factors in the use of these components. Zhang et al. (*47*) demonstrated in their research that the fatigue resistance of 316 L steel following UNSM results from the synergistic effects of reduced surface and subsurface defects, as well as the presence of a gradient nanostructure. In fact, they confirmed that UNSM enhances fatigue properties simultaneously by improving surface integrity and creating a gradient microstructure beneath the surface.

Another point that can be deduced from the examination of Fig. 5 is that the increase in test force has resulted in an increase in the average calculated coefficient of friction in both conditions. This seems reasonable because of the increase in surface adhesion and surface contact that occurs when testing at a higher force. In addition, applying a higher force can cause deformation of the surface and potentially lead to heat generation during the test. This in turn can increase the coefficient of friction.

Figure 6 presents the wear rate values obtained by calculation using Eq. [2] for both the as-built and UNSM specimens. The results from the figure clearly show a significant reduction in wear rate after application of the UNSM treatment for both test loads. It is important to note that the rate of wear reduction according to UNSM for forces of 10 and 20 N was 37% and 30%, respectively. This suggests that the wear rate is reduced by an almost similar amount under different test conditions and that the reduction in wear rate is not dependent on the test condition. The primary reason for the reduction in the wear rate in the UNSM sample is

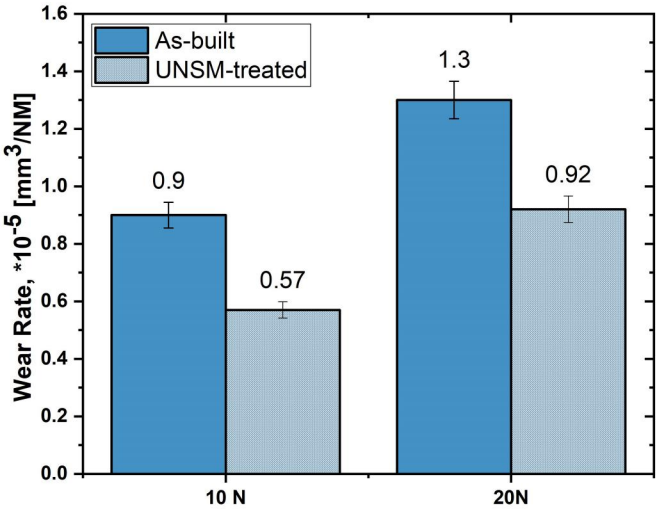

Figure 6. Calculated wear rate in the wear test for the as-built condition and the ultrasonic nanocrystal surface modification (UNSM) condition at two test loads of 10 and 20 Newtons.

the observed increase in hardness, as illustrated in Fig. 3. This increase in hardness is a direct consequence of the reduction in grain size in the surface layer of the UNSM treated sample. Additionally, researchers have noted that decreasing the surface area can lower the rate of wear. (*32*, *57*) In other words, the reduction in surface roughness (Fig. 4) and coefficient of friction (Fig. 5) after UNSM can be another reason for reducing the wear rate, as surface roughness increases the area in contact with the worn surfaces. Previous studies have demonstrated that the application of compressive residual stress, induced by the impact of ultrasonic vibrations on the surface, can effectively reduce the wear rate. (*58*)

Figure 7 displays the weight reduction graph for both as-built and UNSM samples. The graph illustrates the relationship between distance and weight reduction under two forces: 10 and 20 N. It can be seen in both graphs that the weight loss curve of the modified sample is at a lower level than that of the unmodified sample. This demonstrates that surface modification of the specimen improves the wear resistance of the Inconel 625 alloy. For example, the figure shows that at a test load of 10 N, the modified sample achieves the same mass loss as the unmodified sample at 1,000 meters, but at 1400 meters. The same result was observed when a test force of 20 N was applied, although the weight loss values were higher with the greater force. As mentioned in the interpretation of the wear rate results obtained, the UNSM treatment can create fine microstructures on the sample surface. These microstructures can enhance wear resistance by increasing hardness. Furthermore, the manufacturing process may introduce tensile surface stresses, which can lead to microcracking of the specimen surface (*59*) and increase its susceptibility to wear.

However, the UNSM treatment effectively mitigates these tensile stresses by applying compressive stresses instead. These compressive residual stresses counteract the formation and propagation of cracks, thereby improving wear resistance. Previous studies on various alloys have comprehensively documented this phenomenon, indicating that compressive stresses significantly improve the wear properties of metallic surfaces. (*58*,*60*,*61*)

It should also be noted that increasing the test load may result in an increase in weight loss. This is because the higher test load can result in more plastic deformation on the sample surface during testing. This deformation can cause microcracking and spalling of the specimen surface, reducing the wear resistance. This is confirmed by the results shown in Fig. 7(b). Increasing the normal force also causes more wear particles to separate and strike the surface of the specimen. This can further increase the amount of weight lost during wear.

Figure 8 shows the results of the structural changes in the alloy after UNSM treatment. It can be observed in Fig. 8a that the dominant phase present in the structure is the γ phase, which is essentially a solid solution composed of nickel, chromium and iron elements. The formation of the γ phase as the major phase in the structure of Inconel 625 alloy has been reported in previous research. (*1*,*2*) This

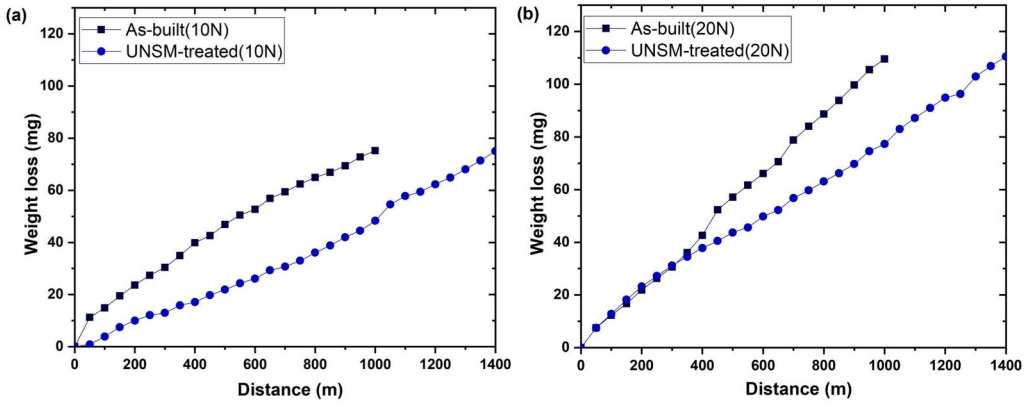

Figure 7. Graph showing the loss of mass versus distance in the wear test for both the as built and ultrasonic nanocrystal surface modification (UNSM) treated samples under a test load of 10 Newtons (a) and 20 Newtons (b).

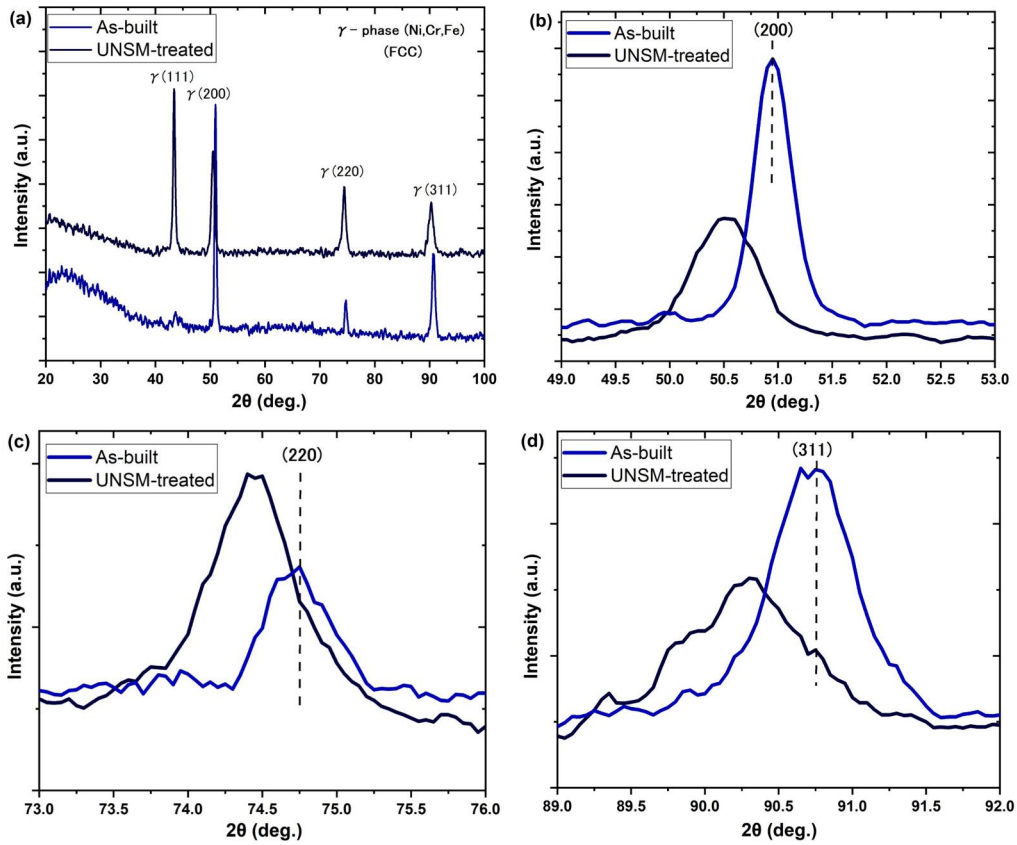

Figure 8. XRD graph comparing the as-built and ultrasonic nanocrystal surface modification (UNSM) treated samples (a) and higher magnification images of the three main peak locations in the two samples for clearer comparison (b, c and d).

finding is consistent with the phase balance obtained from the Nickel-Chromium-Iron (Ni-Cr-Fe) ternary diagram. (*62*)

However, closer examination of the X-ray diffraction pattern in both the as-built and UNSM treated specimens reveals that the location of the phase peaks has changed slightly after the surface treatment. Figure 8b–d show the peaks corresponding to crystal planes (200), (220), and (311) respectively at higher magnification. As can be seen from these figures, at all these peaks the UNSM curve (black curve) has shifted to the left compared to the as-built curve (blue curve). This can be interpreted in terms of the strain imposed on the structure by the surface treatment. Before delving into the quantitative calculation of lattice strain presented below, it is important to note that the left shift of the peaks indicates the application of uniform strain in the crystal structure. Previous studies have shown that when lattice strain is generated uniformly within a structure, it leads to the phenomenon of an expanding unit cell. (*63*) As a result, the distance between crystal planes increases, causing the diffraction angle to decrease and shift to lower values in accordance with the Bragg's law relation. (*64*) The results obtained in this research are consistent with this point,

indicating that after the UNSM treatment the main peaks of the gamma phase have shifted to the left. In a study of the effect of UNSM on the properties of AISI 4340 materials, it was also reported that the XRD peaks were shifted to the left. (52)

Furthermore, the lattice strain on the surface was investigated using the Uniform Deformation Model (UDM) proposed by Williamson-Hall, (65) based on the results of the XRD analysis. Peak broadening in XRD analysis is influenced by two main factors: crystallite size reduction and lattice strain. Crystallite size reduction results in a broader peak because smaller crystallites cause more diffraction broadening. (66) Conversely, lattice strain distorts the crystal lattice, causing variations in d-spacing and resulting in peak broadening. (67) This can be expressed as:

$$\beta_{hkl} = \beta_D + \beta_\varepsilon$$

where β_D is the peak broadening due to crystallite size contribution, β_ε is the peak broadening due to strain, and β_{hkl} is the full width at half maximum (FWHM). The relationship between β_D and the average crystallite size can also be obtained using the Debye-Scherrer equation:

$$D = \frac{k\lambda}{\beta_D \cos\theta}$$

where the constant K is equal to 0.90, λ is the wavelength of the X-ray with the copper source ($\lambda = 0.5406$ nm), D is the crystallite size and θ is the Bragg angle. crystallite size (or domain size) refers to the size of coherent, diffracting domains within a grain. These crystallites are regions within the grain that are free from internal defects such as dislocations and grain boundaries. (68) The measured results for the FWHM parameter and the calculated results for the crystallite size are presented in Table 1. The results obtained from all three main peaks consistently demonstrate that the FWHM value increased after surface treatment. Given the direct relationship between the increase in peak width and the decrease in crystallite size, this confirms that the UNSM treatment has resulted in the formation of a finer structure. The calculated results shown in the table confirm that the crystal size has decreased due to the UNSM treatment, again indicating a refinement in the structure.

It has been reported that instrument effects can cause changes in the FWHM parameter of 0.06° to 0.09°. (69) However, it should be noted that for all peaks, the increase in peak width progressed from as-built to UNSM, and at no point did the as-built peak become wider than the UNSM peak under random conditions. Additionally, this increase also resulted in an angular change of more than 0.06° to 0.09° across all peaks. Therefore, it seems reasonable to assume that the broadening of the UNSM peaks could be a result of lattice changes, including a decrease in crystallite size.

It should be noted that the application scope for grain size in the Scherrer equation should not exceed 200 nm due to the limitations of diffractometer resolution. (70) As indicated in previous microstructure images, the very fine grains formed in the SLM alloy—resulting from the high solidification rate—became even finer in the UNSM region, with sizes approximately 100 nm (Fig. 1d and h). Therefore, applying the Scherrer equation to calculate crystallite size is appropriate.

To calculate the lattice strain caused by the UNSM treatment, it is important to note that the peak broadening resulting from the strain is directly related to the amount of lattice strain:

$$\beta_\varepsilon = \varepsilon \text{ta n}\theta$$

In this context, ε represents the strain and θ refers to the peak position in radians. Substituting the values from the previous equations into the given relationship, we obtain the following relationship:

$$\beta_{\text{hkl}} \cos\theta = \frac{k\lambda}{D} + \varepsilon \sin\theta$$

Since the full width at half maximum can be determined from the XRD results, a graph can be plotted. The vertical axis of the graph represents the $\beta_{\text{hkl}}\cos\theta$ values while the horizontal axis represents the $\sin\theta$ values for each of the peaks identified in the XRD graph. In such a graph, ε can be calculated by determining the slope of the line obtained from the linear fit of the data. The fitting results for the XRD graph of the as-built and UNSM treated samples are displayed in Fig. 9. The results of linear fitting for lattice strain before and after UNSM treatment were calculated as 0.51 and 0.73, respectively. This result indicates a significant

Table 1. Full width at half maximum and crystallite size parameters calculated in two states: as-built and UNSM treated.

Diffraction peaks	Samples	2Θ degree	FWHM	Crystallite Size, nm
Peak (200)	As-built	50.95	0.36	8.58
	UNSM-treated	50.51	0.68	4.53
Peak (220)	As-built	74.73	0.46	7.62
	UNSM-treated	74.42	0.67	5.22
Peak (311)	As-built	90.73	0.68	5.83
	UNSM-treated	90.28	1.2	3.87

Abbreviation: UNSM, Ultrasonic nanocrystal surface modification.

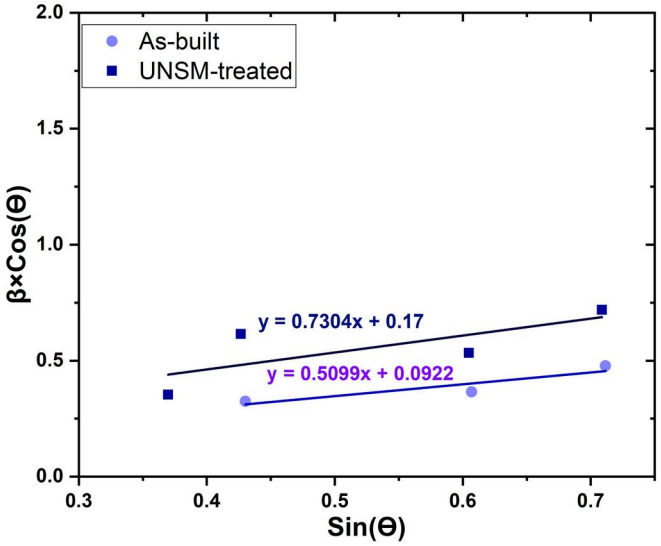

Figure 9. The plot shows the changes in βhkl.cosθ as a function of sinθ for the main peaks in the X-ray diffraction pattern of the Inconel 625 alloy in both as-built and ultrasonic nanocrystal surface modification (UNSM) treated conditions. The results are presented together with a linear fit.

increase in lattice strain in the structure following the UNSM surface modification treatment. This finding, in addition to the previous finding of an increase in the distance between the crystal planes (resulting in decreased diffraction angles and shifted peaks to the left), indicates that the lattice strain induced on the surface of the UNSM treated sample was compressive.

Figure 10 shows the SEM images of the surface of the as-built and UNSM treated samples. The SEM images were acquired following the conclusion of the test. Consequently, it is essential to note that, for the UNSM specimen, as mentioned in the explanation of Fig. 6, the wear test was extended to 1,400 meters to achieve a weight loss equivalent to that of the as-built state. It can be seen from this figure that the sliding direction is more clearly visible in the as-built specimen. In contrast, the UNSM treated sample exhibits a greater amount of wear debris and a higher incidence of delamination phenomenon. When interpreting this result, it is important to note that in materials with lower hardness, the plastic deformation capacity is higher, which means that work hardening is also higher. As a result, the deformation paths due to wear are easier to see. This phenomenon can be observed both on a larger scale, as seen in the sliding direction, and on a smaller scale, as seen in the wear tracks of the as-built sample (Fig. 10a and b). However, in a harder material, it becomes more difficult to recognize the paths of plastic deformation or sliding direction, as well as wear tracks. This is because the capacity for plastic deformation is reduced in materials with higher hardness, also known as lower work hardenability. (*71*) This reduction in capacity for plastic deformation is evidenced by the increase in debris formation on the sides of the wear paths and the higher level of delamination in the wear path. Both phenomena are observed in the UNSM specimens (Fig. 10c and d). In summary, the increase in hardness of the UNSM sample correlates with a decrease in work hardenability, which heightens the risk of delamination during pin movement. Nonetheless, this does not imply a corresponding increase in weight loss. For instance, a material such as the as-built sample, characterized by lower hardness and greater susceptibility to plastic deformation, may experience greater material loss along the wear path due to more effective sliding and cutting. Furthermore, it is important to note that, as previously mentioned, SEM images of the UNSM sample taken after

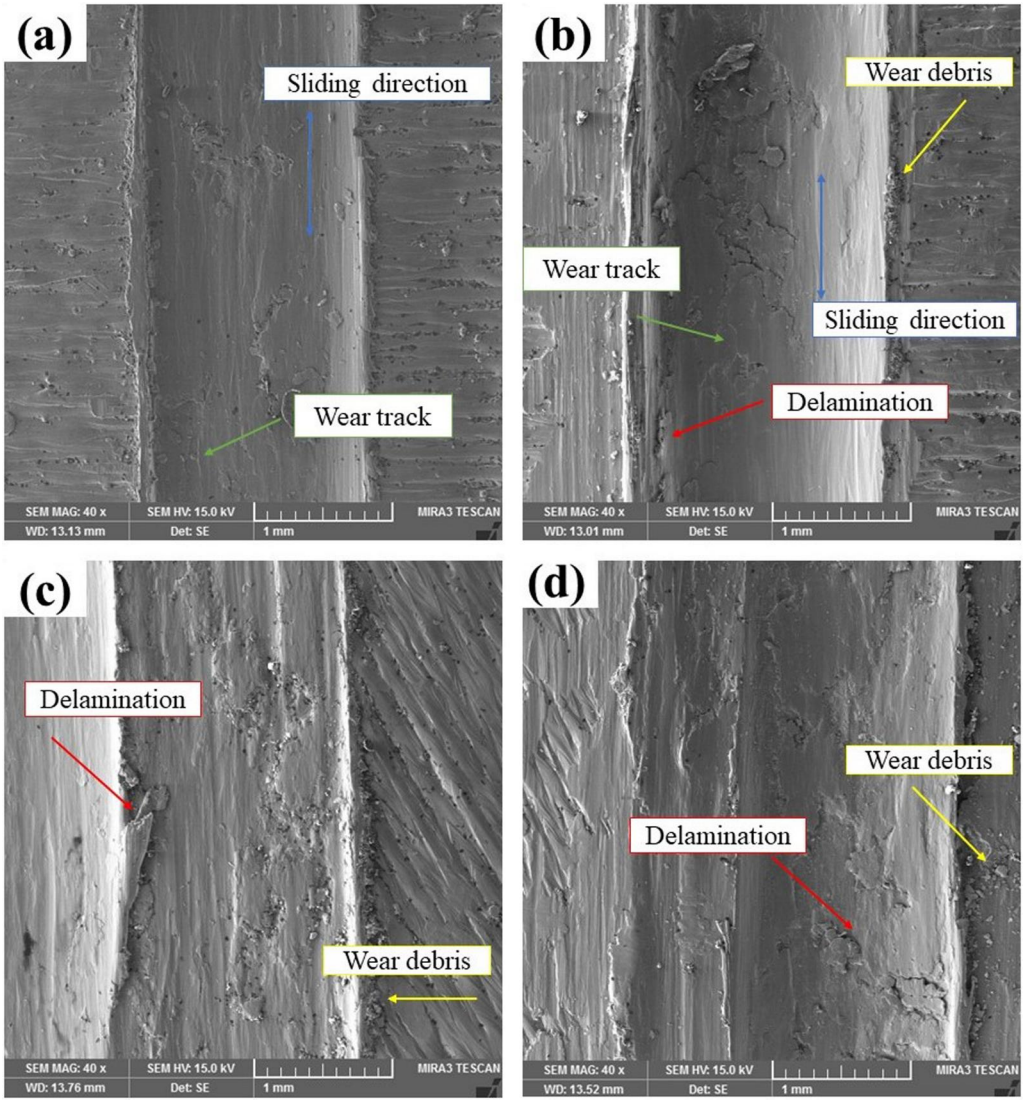

Figure 10. Worn surface of Inconel 625 alloy in as-built condition (a and b) and ultrasonic nanocrystal surface modification (UNSM) treated condition (c and d).

1,400 m—at which point the weight loss was equivalent to that of the as-built sample after 1,000 m—are included. Consequently, the increased delamination may also be attributed to the extended wear distance encountered by the UNSM sample.

The images in Fig. 10 therefore confirm that the difference in wear behavior between the as-built and UNSM specimens is due to the difference in hardness and work hardenability of the respective specimens. In other words, examination of the wear path by SEM revealed that the UNSM treatment had improved hardness and wear resistance in a limited area of the surface by reducing work hardenability.

Figure 11 shows higher magnifications of the areas inside the wear track at two different forces in the UNSM treated sample. The main observation in both samples is the formation of debris. This debris is a consequence of the failure of the harder sample when it undergoes plastic deformation due to wear. This was also mentioned in the interpretation of the previous figure: due to the increase in hardness and the decrease in the material's ability to work hardening, more debris is created in the UNSM treated sample. Another important point to note is that as the force increases, cracks can also be observed in the delamination areas (Fig. 11b). This finding is consistent with the results obtained in Fig. 10 and shows a reduction in work hardenability in the UNSM sample. With the increase in hardness and decrease in work hardenability, together with an increase in the amount of test load that increases the strain rate, the behavior of the material becomes more brittle. As a result, cracks are observed in the UNSM specimen in the wear path and in the delamination regions when a force of 20 Newtons is applied.

Figure 12 can also be used to check the wear mechanism. This figure displays images of the wear paths in both the as-built and UNSM treated samples using two secondary and backscattered electron detectors. It is clear from these images that both adhesive and abrasive mechanisms are present in both the as-built and UNSM samples. However, it is noteworthy that the areas of abrasive wear are more pronounced in each sample, suggesting that abrasive wear is the predominant mechanism. In other words, the surface modification on the alloy did not alter the wear mechanism. This is evident from the presence of plastic deformation and extensive damage observed in the wear path in both the as-built and UNSM-treated conditions. The adhesive wear

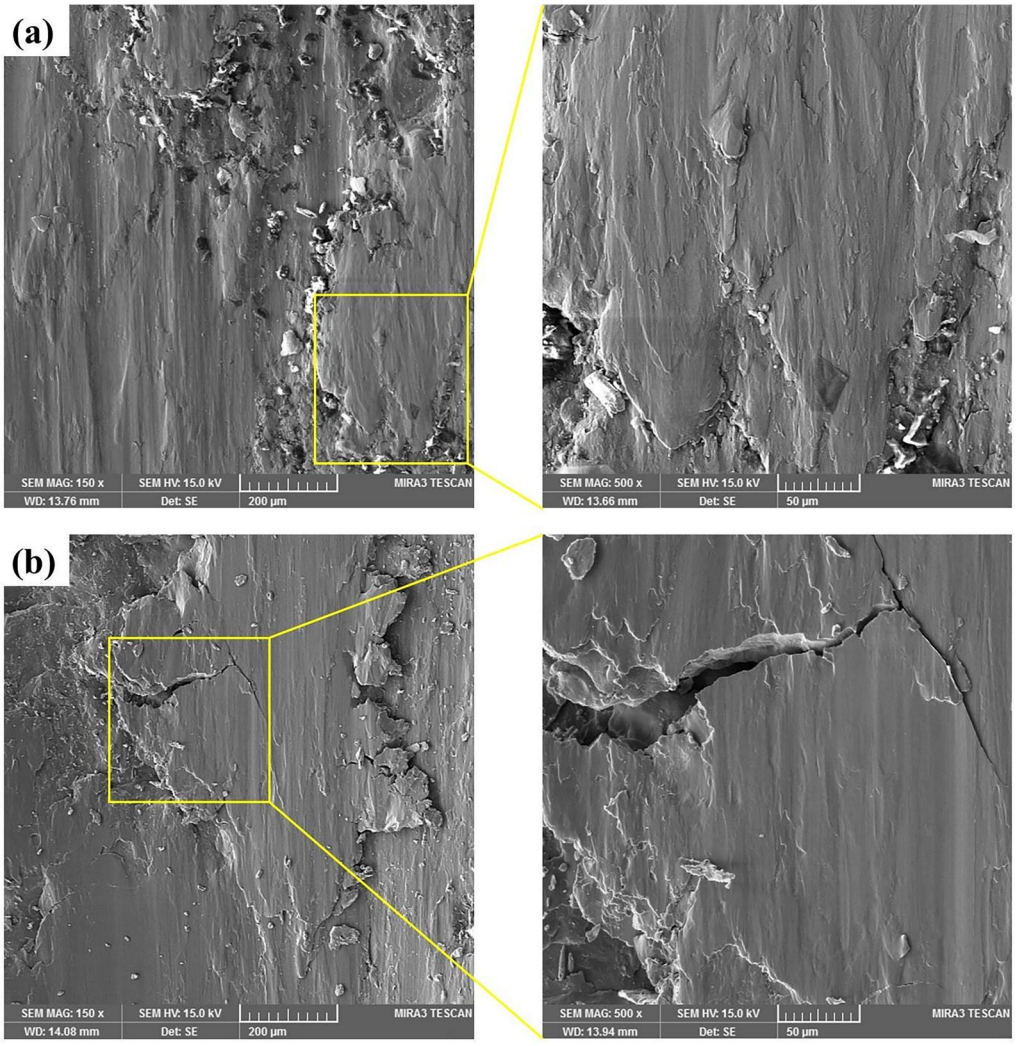

Figure 11. Images of the inside of the wear track of the ultrasonic nanocrystal surface modification (UNSM) treated sample under a test load of 10 Newtons (a) and 20 Newtons (b).

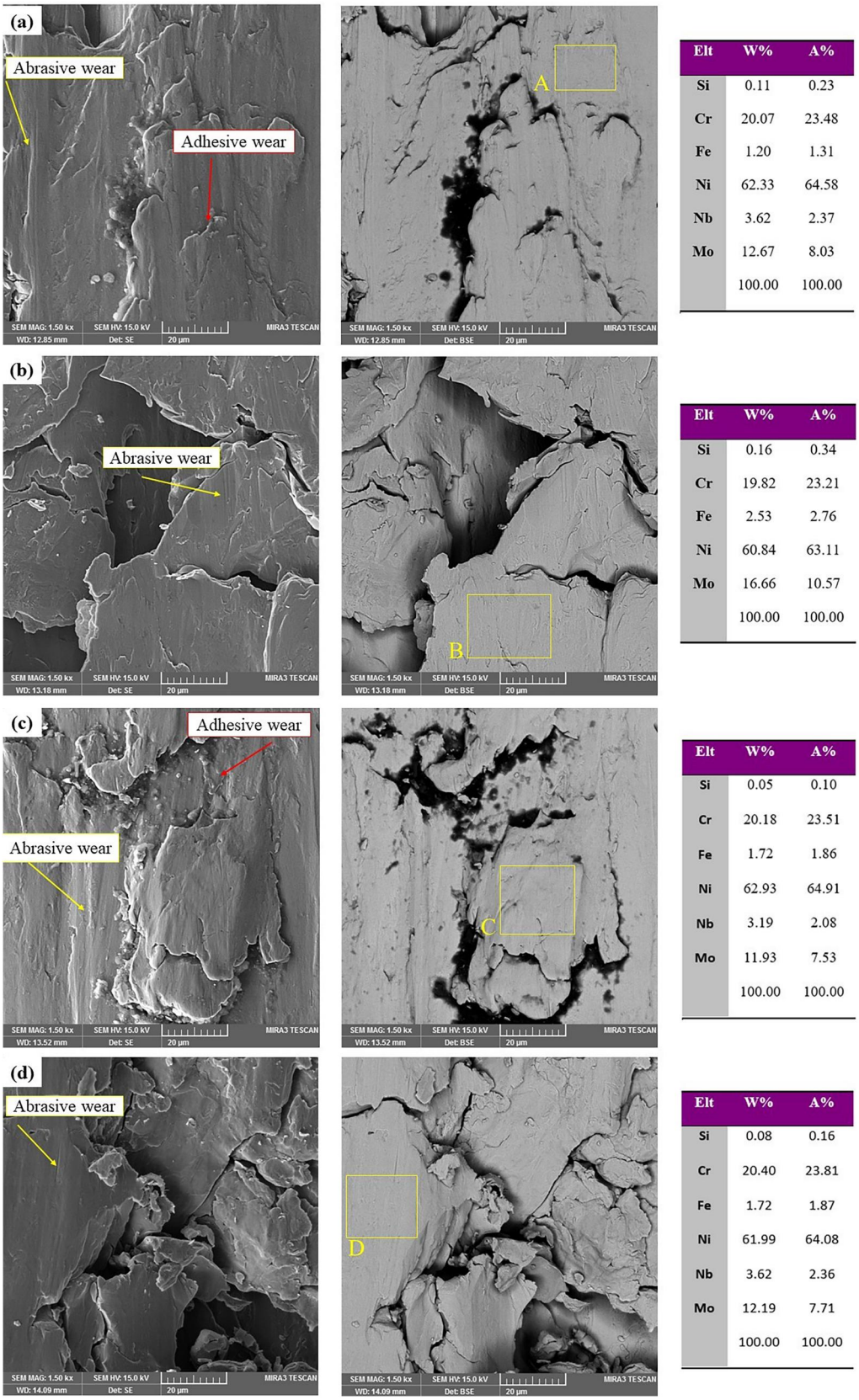

Elt	W%	A%
Si	0.11	0.23
Cr	20.07	23.48
Fe	1.20	1.31
Ni	62.33	64.58
Nb	3.62	2.37
Mo	12.67	8.03
	100.00	100.00

Elt	W%	A%
Si	0.16	0.34
Cr	19.82	23.21
Fe	2.53	2.76
Ni	60.84	63.11
Mo	16.66	10.57
	100.00	100.00

Elt	W%	A%
Si	0.05	0.10
Cr	20.18	23.51
Fe	1.72	1.86
Ni	62.93	64.91
Nb	3.19	2.08
Mo	11.93	7.53
	100.00	100.00

Elt	W%	A%
Si	0.08	0.16
Cr	20.40	23.81
Fe	1.72	1.87
Ni	61.99	64.08
Nb	3.62	2.36
Mo	12.19	7.71
	100.00	100.00

Figure 12. Images of the as-built and ultrasonic nanocrystal surface modification (UNSM) treated specimens with the secondary electron and backscatter electron detectors, respectively, under test forces of 10 N and 20 N. The images are labeled (a) and (b) for the as-built specimens and (c) and (d) for the UNSM treated specimens.

mechanism typically involves the formation of strong adhesive bonds at the asperities of the contacting surfaces, leading to material transfer and potential surface damage. Abrasive wear, in contrast, is characterized by the removal of material through mechanical action, often involving hard particles or rough asperities. This type of wear can cause

surface deformation, generate wear debris, and, in some cases, lead to a brittle fracture, resulting in smooth and elongated wear tracks. In both samples, signs of abrasive wear were observed across larger areas. This observation aligns with previous studies, which have identified abrasive wear as the primary mechanism in Inconel 625 alloy (*43,72*)

The backscattered electron images next to the secondary electron images also show that there is no phase change in the microstructure during wear. This is important because the formation of second phases, including oxide phases, can directly affect wear mechanisms. Comparing the analyses of two points A and B with points C and D reveals that the surface treatment applied to the specimen did not alter the chemical composition of the worn surface. As explained earlier, the variation in wear behavior and rate was due to the change in plastic deformation behavior.

Conclusions

The findings of this study demonstrate that the UNSM process significantly enhances the surface properties of Inconel 625 alloy produced by SLM. The application of UNSM led to a substantial reduction in surface roughness, with the Ra value decreasing from 6.320 to 0.558 µm. This reduction in roughness not only improved wear resistance but also increased surface hardness from approximately 300 Vickers to 500 Vickers. Additionally, the coefficient of friction was markedly reduced from 0.33 to 0.03.

The UNSM treatment also induced notable microstructural changes, including a reduction in crystallite size and an increase in lattice strain from 0.51 to 0.73, contributing to the improved wear resistance of the alloy. As a result, the wear rate of the alloy decreased by 37% and 30% under test forces of 10 Newtons and 20 Newtons, respectively. Furthermore, the wear resistance was significantly enhanced, with the distance to weight loss at a 10 N load extending from 1,000 meters for the as-built alloy to 1,400 meters after UNSM treatment.

These results suggest that UNSM is an effective surface modification technique for enhancing the surface properties of Inconel 625 alloy, particularly in reducing roughness, increasing hardness, and improving wear resistance. To further extend the applicability of this treatment, it is recommended that additional tribological properties of the alloy be evaluated after UNSM implementation.

Disclosure statement

No potential conflict of interest was reported by the author(s).

Funding

Filipe Fernandes acknowledges the: UIDB/00285/2020 and LA/P/0112/2020 projects, sponsored by FEDER Funds through Portugal 2020 (PT2020), by the Competitiveness and Internationalization Operational Program (COMPETE 2020), and national funds through the Portuguese Foundation for Science and Technology (FCT).

ORCID

Morteza Hadi http://orcid.org/0000-0002-9284-7481

References

(1) Li, S., Wei, Q., Shi, Y., Zhu, Z., and Zhang, D. (2015), "Microstructure Characteristics of Inconel 625 Superalloy Manufactured by Selective Laser Melting," *Journal of Materials Science & Technology*, **31**, pp 946–952. doi:10.1016/j.jmst.2014.09.020

(2) Shankar, V., Rao, K. B. S., and Mannan, S. (2001), "Microstructure and Mechanical Properties of Inconel 625 Superalloy," *Journal of Nuclear Materials*, **288**, pp 222–232. doi:10.1016/S0022-3115(00)00723-6

(3) Chen, J., Wang, J., Chen, B., and Yan, F. (2011), "Tribocorrosion Behaviors of Inconel 625 Alloy Sliding against 316 Steel in Seawater," *Tribology Transactions*, 54, pp 514–522. doi:10.1080/10402004.2011.571362

(4) de Oliveira, M. M., Couto, A. A., Almeida, G. F. C., Reis, D. A. P., de Lima, N. B., and Baldan, R. (2019), "Mechanical Behavior of Inconel 625 at Elevated Temperatures," *Metals*, **9**, 301. doi:10.3390/met9030301.

(5) Dinda, G. P., Dasgupta, A. K., and Mazumder, J. (2009), "Laser Aided Direct Metal Deposition of Inconel 625 Superalloy: Microstructural Evolution and Thermal Stability," *Materials Science and Engineering: A*, **509**, pp 98–104. doi:10.1016/j.msea.2009.01.009

(6) Kumar, S. P., Elangovan, S., Mohanraj, R., and Ramakrishna, J. (2021), "A Review on Properties of Inconel 625 and Inconel 718 Fabricated Using Direct Energy Deposition," *Materials Today: Proceedings*, **46**, pp 7892–7906. doi:10.1016/j.matpr.2021.02.566

(7) Sehat, A., Hadi, M., Isfahani, T., and Fernandes, F. (2024), "Comparative Analysis of Microstructural, Compositional, and Grazing Incidence Characteristics of Oxide Scale on 316L Steel: SLM v.s Wrought Conditions," *Journal of Materials Research and Technology*, **31**, pp 2077–2093. doi:10.1016/j.jmrt.2024.06.229

(8) Liu, Y., Zhai, X., Deng, Y., and Wu, D. (2019), "Tribological Property of Selective Laser Melting–Processed 316L Stainless Steel against Filled PEEK under Water Lubrication," *Tribology Transactions*, **62**, pp 962–970. doi:10.1080/10402004.2019.1635671

(9) Gong, L., Pan, Y., Peng, C., Fu, X., Jiang, Z., and Jiang, S. (2022), *Effect of Ultrasonic Nanocrystal Surface Modification on Wear Properties of High-Carbon High-Chromium Steel.* Available at SSRN 4229961.

(10) Leary, M. (2017), "Surface Roughness Optimisation for Selective Laser Melting (SLM): Accommodating Relevant and Irrelevant Surfaces," *Laser Additive Manufacturing*. Woodhead Publishing Series in Electronic and Optical Materials, pp 99–118, Elsevier. https://www.sciencedirect.com/science/article/abs/pii/B978008100433300004X

(11) Vayssette, B., Saintier, N., Brugger, C., Elmay, M., and Pessard, E. (2018), "Surface Roughness of Ti-6Al-4V Parts Obtained by SLM and EBM: Effect on the High Cycle Fatigue Life," *Procedia Engineering*, **213**, pp 89–97. doi:10.1016/j.proeng.2018.02.010.

(12) She, D., Yue, W., Kang, J., Huang, F., Wang, C., and Shen, J. (2018), "Vacuum Tribological Properties of Titanium Enhanced via Ultrasonic Surface Rolling Processing Pretreatment and Plasma Nitriding," *Tribology Transactions*, **61**, pp 612–620. doi:10.1080/10402004.2017.1380870.

(13) Tripathi, K., Gyawali, G., Amanov, A., and Lee, S. W. (2017), "Synergy Effect of Ultrasonic Nanocrystalline Surface Modification and Laser Surface Texturing on Friction and Wear Behavior Of Graphite Cast Iron," *Tribology Transactions*, **60**, pp 226–237. doi:10.1080/10402004.2016.1158339

(14) Ke, L. and Jian, L. (1999), "Surface Nanocrystallization (SNC) of Metallic Materials-Presentation of the Concept Behind a New Approach," *Journal of Materials Sciences and Technology*, **15**, 193.

(15) Wu, B., Wang, P., Pyoun, Y.-S., Zhang, J., and Murakami, R-i (2012), "Effect of Ultrasonic Nanocrystal Surface Modification

on the Fatigue Behaviors of Plasma-Nitrided S45C Steel," *surface and Coatings Technology*, **213**pp 271–277. doi:10.1016/j.surfcoat.2012.10.063.

(16) Wagner, L. (1999), "Mechanical Surface Treatments on Titanium, Aluminum and Magnesium Alloys," *Materials Science and Engineering: A*, **263**, pp 210–216. doi:10.1016/S0921-5093(98)01168-X

(17) Siddaiah, A., Mao, B., Liao, Y., and Menezes, P. L. (2020), "Effect of Laser Shock Peening on the Wear–Corrosion Synergistic Behavior of an az31b Magnesium Alloy," *Journal of Tribology*, **142**, pp 041701. doi:10.1115/1.4045500.

(18) Kumar, S. A., Sundar, R., Raman, S. G. S., Kumar, H., Gnanamoorthy, R., Kaul, R., Ranganathan, K., Oak, S. M., and Kukreja, L. M. (2012), "Fretting Wear Behavior of Laser Peened Ti-6Al-4V," *Tribology Transactions*, **55**, pp 615–623. doi:10.1080/10402004.2012.686087.

(19) Siddaiah, A., Mao, B., Liao, Y., and Menezes, P. L. (2018), "Surface Characterization and Tribological Performance of Laser Shock Peened Steel Surfaces," *Surface and Coatings Technology*, **351**, pp 188–197. doi:10.1016/j.surfcoat.2018.07.087

(20) Han, X., Zhang, Z., Pang, B., Barber, G. C., Zhao, J., and Qiu, F. (2022), "The Effect of Shot-Peening Time on Tribological Behavior of AISI5160 Steel," *Tribology Transactions*, **65**, pp 801–812. doi:10.1080/10402004.2022.2078257.

(21) Kim, M.-s., Oh, W.-j., Baek, G.-y., Jo, Y.-k., Lee, K.-y., Park, S.-h., and Shim, D.-s. (2020), "Ultrasonic Nanocrystal Surface Modification of High-Speed Tool Steel (AISI M4) Layered via Direct Energy Deposition," *Journal of Materials Processing Technology*, **277**, 116420. doi:10.1016/j.jmatprotec.2019.116420.

(22) Amanov, A., Cho, I.-S., Kim, D.-E., and Pyun, Y.-S. (2012), "Fretting Wear and Friction Reduction of CP Titanium and Ti–6Al–4V Alloy by Ultrasonic Nanocrystalline Surface Modification," *Surface and Coatings Technology*, **207**, pp 135–142. doi:10.1016/j.surfcoat.2012.06.046

(23) Zhao, X., Zhao, Y., Xu, D., and Hu, C. (2020), "Effect of Gradient Nanostructure on Plasma Sulfonitrocarburizing of 42MnCr52 Steel," *Tribology Transactions*, **63**, pp 133–143. doi:10.1080/10402004.2019.1664687

(24) Unal, O., Husem, F., Maleki, E., Karademir, I., Efe, Y., and Das, T. (2022), "Effects of Static Load on Microstructural and Mechanical Performance of AISI 1050 Medium Carbon Steel Subjected to Ultrasonic Nanocrystal Surface Modification," *Materials Science and Engineering: A*, **832**, 142489. doi:10.1016/j.msea.2021.142489.

(25) Karimbaev, R. M., Pyun, Y.-S., and Amanov, A. (2022), "Fatigue Life Extension of Additively Manufactured Nickel-Base 718 Alloy by Nanostructured Surface," *Materials Science and Engineering: A*, **831**, 142041. doi:10.1016/j.msea.2021.142041

(26) Magazov, N., Satbaeva, Z., Rakhadilov, B., and Amanov, A. (2023), "A Study on Surface Hardening and Wear Resistance of AISI 52100 Steel by Ultrasonic Nanocrystal Surface Modification and Electrolytic Plasma Surface Modification Technologies," *Materials*, **16**, 6824. doi:10.3390/ma16206824

(27) Zhang, R., Zhao, W., Zhang, H., Yang, W., Wang, G.-X., Dong, Y., and Ye, C. (2021), "Fatigue Performance Rejuvenation of Corroded 7075-T651 Aluminum Alloy through Ultrasonic Nanocrystal Surface Modification," *International Journal of Fatigue*, **153**, 106463. doi:10.1016/j.ijfatigue.2021.106463.

(28) Karimbaev, R. M., Cho, I. S., Pyun, Y. S., and Amanov, A. (2022), "Effect of Ultrasonic Nanocrystal Surface Modification Treatment at Room and High Temperatures on the High-Frequency Fatigue Behavior of Inconel 718 Fabricated by Laser Metal Deposition," *Metals*, **12**, 515. doi:10.3390/met12030515

(29) Ye, C., Telang, A., Gill, A. S., Suslov, S., Idell, Y., Zweiacker, K., Wiezorek, J. M. K., Zhou, Z., Qian, D., Mannava, S. R., and Vasudevan, V. K. (2014), "Gradient Nanostructure and Residual Stresses Induced by Ultrasonic Nano-Crystal Surface Modification in 304 Austenitic Stainless Steel for High Strength and High Ductility," *Materials Science and Engineering: A*, **613**, pp 274–288. doi:10.1016/j.msea.2014.06.114.

(30) Cao, X. J., Pyoun, Y. S., and Murakami, R. (2010), "Fatigue Properties of a S45C Steel Subjected to Ultrasonic Nanocrystal Surface Modification," *Applied Surface Science*, **256**, pp 6297–6303. doi:10.1016/j.apsusc.2010.04.007

(31) Bagherian Azhiri, R., Jadidi, A., Bideskan, A. S., and Dizadji, M. R. (2021), "Ultrasonic Nanocrystalline Surface Modification of Low Strength Aluminum Alloy: Trade-Off Between Surface Integrity and Production Rate Aiming at Desired Fatigue Life," *The International Journal of Advanced Manufacturing Technology*, **113**, pp 1237–1251. doi:10.1007/s00170-021-06617-2.

(32) Amanov, A., Penkov, O. V., Pyun, Y.-S., and Kim, D.-E. (2012), "Effects of Ultrasonic Nanocrystalline Surface Modification on the Tribological Properties of AZ91D Magnesium Alloy," *Tribology International*, **54**, pp 106–113. doi:10.1016/j.triboint.2012.04.024

(33) Amanov, A. (2021), "Effect of Post-Additive Manufacturing Surface Modification Temperature on the Tribological and Tribocorrosion Properties of Co-Cr-Mo Alloy for Biomedical Applications," *Surface and Coatings Technology*, **421**, 127378. doi:10.1016/j.surfcoat.2021.127378

(34) Amanov, A., Kim, J., Pyun, Y., Hirayama, T., and Hino, M. (2015), "Wear Mechanisms of Silicon Carbide Subjected to Ultrasonic Nanocrystalline Surface Modification Technique," *Wear*, **332–333**, pp 891–899. doi:10.1016/j.wear.2014.11.031.

(35) Amanov, A., Pyun, Y.-S., and Sasaki, S. (2014), "Effects of Ultrasonic Nanocrystalline Surface Modification (UNSM) Technique on the Tribological Behavior of Sintered Cu-Based Alloy," *Tribology International*, **72**, pp 187–197. doi:10.1016/j.triboint.2013.12.003

(36) Maleki, E., Unal, O., Guagliano, M., and Bagherifard, S. (2021), "The Effects of Shot Peening, Laser Shock Peening and Ultrasonic Nanocrystal Surface Modification on the Fatigue Strength of Inconel 718," *Materials Science and Engineering: A*, **810**, 141029. doi:10.1016/j.msea.2021.141029

(37) Sidhu, K. S., Shi, J., Vasudevan, V. K., and Mannava, S. R. (2017), "Residual Stress Enhancement in 3D Printed Inconel 718 Superalloy Treated by Ultrasonic Nano-Crystal Surface Modification," International Manufacturing Science and Engineering Conference, Los Angeles, California, USA, American Society of Mechanical Engineers. doi:10.1115/MSEC2017-2918.

(38) Li, K., He, Y., Cho, I. S., Lee, C. S., Park, I. G., Song, J-i., Yang, C.-W., Lee, J.-H., and Shin, K. (2015), "Effect of Ultrasonic Nanocrytalline Surface Modification on the Microstructural Evolution of Inconel 690 Alloy," *Materials and Manufacturing Processes*, 30, pp 194–198. doi:10.1080/10426914.2014.921694.

(39) Li, J., Lu, Y., Zhang, H., and Xin, L. (2015), "Effect of Grain Size and Hardness on Fretting Wear Behavior of Inconel 600 Alloys," *Tribology International*, **81**, pp 215–222. doi:10.1016/j.triboint.2014.08.005

(40) Xin, L., Yang, B. B., Wang, Z. H., Li, J., Lu, Y. H., and Shoji, T. (2016), "Microstructural Evolution of Subsurface on Inconel 690TT Alloy Subjected to Fretting Wear at Elevated Temperature," *Materials & Design*, **104**, pp 152–161. doi:10.1016/j.matdes.2016.05.030.

(41) Kattoura, M., Telang, A., Mannava, S. R., Qian, D., and Vasudevan, V. K. (2018), "Effect of Ultrasonic Nanocrystal Surface Modification on residual stress, microstructure and fatigue behavior of ATI 718Plus alloy," *Materials Science and Engineering: A*, **711**pp 364–377. doi:10.1016/j.msea.2017.11.043.

(42) Koutiri, I., Pessard, E., Peyre, P., Amlou, O., and De Terris, T. (2018), "Influence of SLM Process Parameters on the Surface Finish, Porosity Rate and Fatigue Behavior of As-Built Inconel 625 Parts," *Journal of Materials Processing Technology*, **255**, pp 536–546. doi:10.1016/j.jmatprotec.2017.12.043.

(43) Jeyaprakash, N., Yang, C.-H., Prabu, G., and Clinktan, R. (2022), "Microstructure and Tribological Behaviour of Inconel-625 Superalloy Produced by Selective Laser Melting," *Metals and Materials International*, **28**, pp 2997–3015. doi:10.1007/s12540-022-01198-5.

(44) Yasuoka, M., Wang, P., Zhang, K., Qiu, Z., Kusaka, K., Pyoun, Y.-S., and Murakami, R-i (2013), "Improvement of the Fatigue

Strength of SUS304 Austenite Stainless Steel Using Ultrasonic Nanocrystal Surface Modification," *Surface and Coatings Technology*, **218**, pp 93–98. doi:10.1016/j.surfcoat.2012.12.033.

(45) Basirat, M., Isfahani, T., and Hadi, M. (2024), "Implementing Shear-Punch Test for the Assessment of Mechanical Properties of Cast and Selective Laser Melted AlSi10Mg Alloys," *Progress in Additive Manufacturing*, **9**, pp 2375–2391. doi:10.1007/s40964-024-00592-2.

(46) Kim, M. S., Park, S. H., Pyun, Y. S., and Shim, D. S. (2020), "Optimization of Ultrasonic Nanocrystal Surface Modification for Surface Quality Improvement of Directed Energy Deposited Stainless Steel 316L," *Journal of Materials Research and Technology*, **9**, pp 15102–15122. doi:10.1016/j.jmrt.2020.10.092

(47) Zhang, Y., Peng, L., Ye, Y., Chi, Y., Gao, L., Zha, X., Huang, T., Zhang, Y., Ding, H., and Ye, C. (2025), "Exploring the Strengthening Mechanisms of Additive Manufactured Metals Treated by Ultrasonic Nanocrystal Surface Modification," *International Journal of Fatigue*, **190**, 108609. doi:10.1016/j.ijfatigue.2024.108609.

(48) Amanov, A., Karimbaev, R., Maleki, E., Unal, O., Pyun, Y.-S., and Amanov, T. (2019), "Effect of Combined Shot Peening and Ultrasonic Nanocrystal Surface Modification Processes on the Fatigue Performance of AISI 304," *Surface and Coatings Technology*, **358**, pp 695–705. doi:10.1016/j.surfcoat.2018.11.100.

(49) Ma, C., Dong, Y., and Ye, C. (2016), "Improving Surface Finish of 3D-Printed Metals by Ultrasonic Nanocrystal Surface Modification," *Procedia CIRP*, 45, pp 319–322. doi:10.1016/j.procir.2016.02.339

(50) Sanseong, C., Ro, J.-S., Pyoun, Y.-S., and Amanov, A. (2020), "Effects of High-Temperature UNSM Treatment on Wear Resistance of Ti-6Al-4V Alloy Prepared by Selective Laser Melting.," *Tribology and Lubricants*, **36**, pp 47–54.

(51) Amanov, A. (2020), "Effect of Local Treatment Temperature of Ultrasonic Nanocrystalline Surface Modification on Tribological Behavior and Corrosion Resistance of Stainless Steel 316L Produced by Selective Laser Melting," *Surface and Coatings Technology*, **398**, 126080. doi:10.1016/j.surfcoat.2020.126080

(52) Karimbaev, R., Pyun, Y.-S., Maleki, E., Unal, O., and Amanov, A. (2020), "An Improvement in Fatigue Behavior of AISI 4340 Steel by Shot Peening and Ultrasonic Nanocrystal Surface Modification," *Materials Science and Engineering: A*, **791**, 139752. doi:10.1016/j.msea.2020.139752.

(53) Krolczyk, G. M. and Legutko, S. (2014), "Experimental Analysis by Measurement of Surface Roughness Variations in Turning Process of Duplex Stainless Steel," *Metrology and Measurement Systems*, **21**, pp 759–770. doi:10.2478/mms-2014-0060.

(54) Biffi, C. A., Bassani, P., Nematollahi, M., Shayesteh Moghaddam, N., Amerinatanzi, A., Mahtabi, M. J., Elahinia, M., and Tuissi, A. (2019), "Effect of Ultrasonic Nanocrystal Surface Modification on the Microstructure and Martensitic Transformation of Selective Laser Melted Nitinol," *Materials*, **12**, 3068. doi:10.3390/ma12193068.

(55) Mostajeran, A., Shoja-Razavi, R., Hadi, M., Erfanmanesh, M., and Karimi, H. (2020), "Wear Behavior of Laser Cladded WC-FeAl Coating on 321 Stainless Steel Substrate," *Journal of Laser Applications*, **32**, 1–9. doi:10.2351/7.0000219.

(56) Adivi, H. G., Ebrahimzadeh, I., Hadi, M., and Tayebi, M. (2020), "The Effect of Alumina Nanoparticles Addition on High-Temperature Wear Behavior of Intermetallic Iron Aluminide Produced by the Spark Plasma Sintering Process," *Surface Review and Letters*, **27**, 2050004. doi:10.1142/S0218625X20500043.

(57) Mostajeran, A., Shoja-Razavi, R., Hadi, M., Erfanmanesh, M., Barekat, M., and Savaghebi Firouzabadi, M. (2020), "Evaluation of the Mechanical Properties of WC-FeAl Composite Coating Fabricated by Laser Cladding Method," *International Journal of Refractory Metals and Hard Materials*, **88**, 105199. doi:10.1016/j.ijrmhm.2020.105199.

(58) Amanov, A. and Umarov, R. (2018), "The Effects of Ultrasonic Nanocrystal Surface Modification Temperature on the Mechanical Properties and Fretting wear resistance of Inconel 690 Alloy," *Applied Surface Science*, **441**, pp 515–529. doi:10.1016/j.apsusc.2018.01.293

(59) Hadi, M., Bayat, O., Sadeghi, M., and Isfahani, T. (2022), "Effect of Solution Treatment on the Rollability of a Cu-Ni-Mn-Sn Alloy," *Iranian Journal of Materials Science and Engineering*, **19**, pp 1–11.

(60) Zhao, W., Liu, D., Chiang, R., Qin, H., Zhang, X., Zhang, H., Liu, J., Ren, Z., Zhang, R., Doll, G. L., Vasudevan, V. K., Dong, Y., and Ye, C. (2020), "Effects of Ultrasonic Nanocrystal Surface Modification on the Surface Integrity, Microstructure, and Wear Resistance of 300M Martensitic Ultra-High Strength Steel," *Journal of Materials Processing Technology*, **285**, 116767. doi:10.1016/j.jmatprotec.2020.116767.

(61) Efe, Y., Karademir, I., Husem, F., Maleki, E., Karimbaev, R., Amanov, A., and Unal, O. (2020), "Enhancement in Microstructural and Mechanical Performance of AA7075 Aluminum Alloy via Severe Shot Peening and Ultrasonic Nanocrystal Surface Modification," *Applied Surface Science*, **528**, 146922. doi:10.1016/j.apsusc.2020.146922.

(62) Yen, Y.-w., Su, J.-w., and Huang, D.-p. (2008), "Phase Equilibria of the Fe–Cr–Ni Ternary Systems and Interfacial Reactions in Fe–Cr Alloys with Ni Substrate," *Journal of Alloys and Compounds*, **457**, pp 270–278. doi:10.1016/j.jallcom.2007.03.053

(63) Nasiri-Tabrizi, B. (2014), "Thermal Treatment Effect on Structural Features of Mechano-Synthesized Fluorapatite-Titania Nanocomposite: A Comparative Study," *Journal of Advanced Ceramics*, **3**, pp 31–42. doi:10.1007/s40145-014-0090-4.

(64) Hadi, M., Rafiaei, S. M., and Fernandes, F. (2023), "The Effect of Mo2C Additions on the Oxidation Resistance of (Ti, W) CN Cermets as Base Material for the Production of Cutting Tools," *Ceramics International*, **49**, pp 21538–21545. doi:10.1016/j.ceramint.2023.03.288

(65) Ungár, T. (2001), "Dislocation Densities, Arrangements and Character from X-Ray Diffraction Experiments," *Materials Science and Engineering: A*, **309–310**, pp 14–22. doi:10.1016/S0921-5093(00)01685-3.

(66) Rafiaei, S. M., Hadi, M., and Fernandes, F. (2024), "Synthesis of (Ti, W, Mo) CN Based Cermets with Different Carbides Configurations for Demanding Applications: Study of the Crystal Structure, Microstructure, and Mechanical Properties," *Ceramics International*, **50**, pp 23264–23274. doi:10.1016/j.ceramint.2024.04.050

(67) Bindu, P. and Thomas, S. (2014), "Estimation of Lattice Strain in ZnO Nanoparticles: X-Ray Peak Profile Analysis," *Journal of Theoretical and Applied Physics*, **8**, pp 123–134. doi:10.1007/s40094-014-0141-9.

(68) Ares, J., Pascual, A., Ferrer, I., and Sánchez, C. (2005), "Grain and Crystallite Size in Polycrystalline Pyrite Thin Films," *Thin Solid Films*, **480–481**, pp 477–481. doi:10.1016/j.tsf.2004.11.064.

(69) He, K., Chen, N., Wang, C., Wei, L., and Chen, J. (2018), "Method for Determining Crystal Grain Size by X-Ray Diffraction," *Crystal Research and Technology*, **53**, 1700157. doi:10.1002/crat.201700157.

(70) Cullity, B. and Stock, S. (2001), *Elements of X-Ray Diffraction*, Prentice Hall: Manhattan, USA.

(71) Boroumand, K., Hadi, M., and Vafaei, R. (2021), Hot Deformation Behavior and Constitutive Modelling of a Medium-Carbon Structural Steel. *Physics of Metals and Metallography* **122**(14), pp. 1611–1620. doi:10.1134/S0031918X21140052.

(72) Ferraresi, R., Avanzini, A., Cecchel, S., Petrogalli, C., and Cornacchia, G. (2022), "Microstructural, Mechanical, and Tribological Evolution under Different Heat Treatment Conditions of Inconel 625 Alloy Fabricated by Selective Laser Melting," *Advanced Engineering Materials*, **24**, 2100966. doi:10.1002/adem.202100966.